IEEE Access
Multidisciplinary | Rapid Review | Open Access Journal

SPECIAL SECTION ON EMERGING TRENDS OF ENERGY AND SPECTRUM HARVESTING TECHNOLOGIES

Received November 9, 2020, accepted November 18, 2020, date of publication November 24, 2020, date of current version December 10, 2020.

*Digital Object Identifier 10.1109/ACCESS.2020.3040197*

# Analytical Modeling and Performance Study of A Piezoelectric Laminated Annular Plate for Rotary Energy Harvesting

**TIANYUN GUO[1], ZHIKE XU[1], LEI HUANG[1], MINQIANG HU[1,2], LONG JIN[1], AND JIANHUA WANG[1], (Member, IEEE)**

[1]School of Electrical Engineering, Southeast University, Nanjing 210096, China
[2]School of Electrical and Automation, Nanjing Normal University, Nanjing 210097, China

Corresponding author: Zhike Xu (xuzhike@seu.edu.cn)

This work was supported in part by Chinese National Natural Science Foundation under Grant 51777029, in part by High-Tech Ship Scientific Research Project of the Ministry of Industry and Information Technology under Grant MC-201714-P02, and in part by the Natural Science Foundation of Jiangsu Province under Grant BK20181283.

**ABSTRACT** A piezoelectric energy harvester based on the standing wave vibration of a piezoelectric laminated annular plate is proposed in this article. It can convert the rotary energy into the standing wave vibration energy of the piezoelectric laminated annular plate, and then the standing wave vibration of the thin plate can be directly converted to electrical energy through direct piezoelectric effect of the piezoelectric ceramics. The idea of utilizing the standing wave vibration of the thin plate for rotary energy harvesting is novel according to the existing literature. The proposed structure is particularly suitable for rotating mechanical energy harvesting for its simple structure, convenient installation and high power density. In this article, the energy harvesting structure is introduced in details, the analytical modeling is established to predict the steady-state output features of the energy harvester, and is verified by the finite element analysis (FEA) results as well.

**INDEX TERMS** Piezoelectric laminated annular plate, standing wave vibration, rotary energy harvesting.

## I. INTRODUCTION

Energy harvesting attracts the worldwide attention since it can provide an effective solution to power source for wireless sensor network (WSN) nodes. Among different energy conversion methods, piezoelectric energy harvesting technology is most popular for the merits of simple structure, no heat, no electromagnetic interference, high output voltage, high power density and easy to manufacture [1], [2].

Generally speaking, research on piezoelectric energy harvesting structures can be divided into two directions by whether it works in the resonant state or not [33]. For the resonant state applications, the cantilever structure is most popular for its low eigen-frequency which is desirable for ambient vibrational energy harvesting [1]–[9]. While for the non-resonant applications, the structure usually needs a high tolerance of force load, and the most popular structure is the cymbal transducer [10]–[14]. However, the two popular structures mentioned above are usually applied to linear vibrational energy harvesting, and can't be used for rotary energy harvesting directly.

Rotary energy harvesting technology deserves to be investigated since rotating energy is a kind of ambient abundant mechanical energy. Most of the existing piezoelectric structures which can be utilized for rotary energy harvesting are based on cantilever beams [16]–[20]. The piezoelectric cantilever beam array was installed in the circumferential direction. Mechanism devices are required to apply impact or magnetic force on the cantilever array for excitation purpose. The installation of a limiter is also necessary to avoid the amplitude of the cantilever beam exceeding the piezoelectric ceramic's bearing range [15]. Therefore, this kind of rotary piezoelectric generator is relatively complicated which is a barrier to minimize the harvester.

Studies on plate based piezoelectric energy harvester are very limited [21]–[23], not to mention the plate based structure for rotary energy harvesting. The only related structure utilizes the deformation of the piezoelectric circular plate

The associate editor coordinating the review of this manuscript and approving it for publication was Guangjie Han.

caused by the interaction of the magnets mounted on the thin piezoelectric plate and the bearing cap [24]. This structure realizes the direct conversion from rotating mechanical energy to electrical energy, but its power generation efficiency is quite low due to charge cancellation in piezoelectric materials. Moreover, the output electrical waveform is random, which is not conducive to the design of energy harvesting circuits and the effective utilization of electrical energy.

Charge cancellation can affect the performance of the energy harvester greatly, however, little research has been done on the influence of charge cancellation in both beam and plate based energy harvesting structures. Charge cancellation phenomenon was discovered by Kim *et al.* in 2005. A circular piezoelectric plate clamped on its outer edge would not produce any charge on the electrodes due to its boundary condition. This problem is solved by regrouping the electrodes and dividing the piezoelectric layer into two concentric parts with opposite polarization directions [36]. In 2009, Erturk *et al.* proposed an approach to avoid charge cancellation by using segmented electrode pairs with consideration to the effects of both electrode configurations and strain nodes of the cantilever beam piezoelectric energy harvester with various boundary conditions [37]. In 2014, Aridogan *et al.* investigated the dynamic strain distribution of rectangular plate with all-four-edges clamped boundary condition in order to figure out the optimal position of the piezoelectric patch, they pointed out that vibration mode shapes as well as strain distribution should be taken into consideration for piezoelectric patch positioning [21]. In 2018, Krishnasamy developed two distributed parameter models for a cantilever piezoelectric energy harvester in which the piezoelectric layers were segmented according to the strain nodes of the concerned vibration mode. They proposed two models to deal with different interfaces with the resistive loads [38]. According to existing literature, charge cancellation can be averted by segmenting the piezoelectric layers with proper electrode configuration in the light of the strain distribution and vibration mode.

In this article, a piezoelectric laminated annular plate energy harvester (PLAPEH) is proposed innovatively for rotary energy harvesting based on standing wave vibration. The electrical energy generated by this structure is relatively regular. The electromechanical conversion efficiency and the power density of the harvester are improved by suitable partition and polarization of the piezoelectric layer, as well as corresponding electrode configuration matching with the standing wave vibration mode. This structure can be installed on the shaft of rotating mechanisms to supply power for the health monitoring electronics.

## II. STRUCTURE DIAGRAM AND ANALYSIS PROCESS

The front view, top view and partial cutaway view of PLAPEH are shown in Figure 1. In the figure, 1 is the central fixed shaft, 2 is the flange coupling, 3 is the fastening screw, 4 is the fastening bolt, 5 is the rubber washer, 6 is the

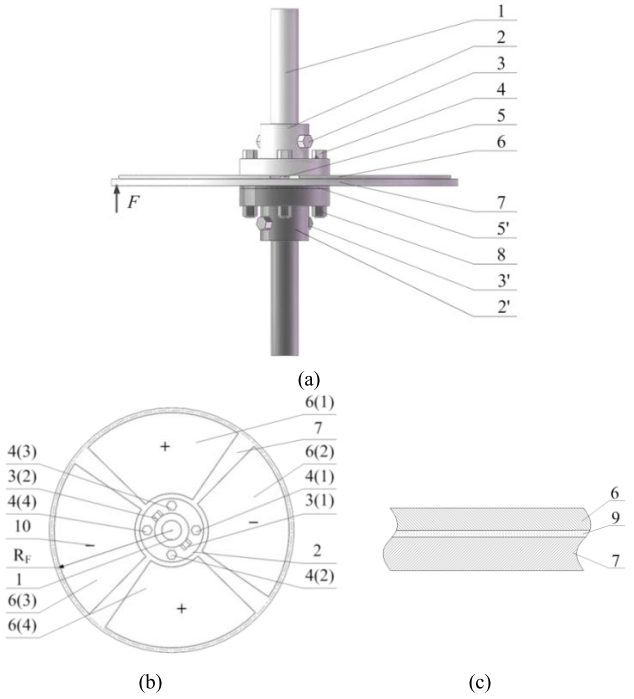


**FIGURE 1.** Front view (a), top view (b) and partial-cutaway view (c) of PLAPEH.

piezoelectric ceramic layer 7 is the metal substrate disc, 8 is the fastening nut, 9 is the epoxy conductive adhesive, 10 is the electrode, $F$ is the transverse point-wise force.

A piezoelectric laminated annular plate and a central fixed shaft are two main parts of the proposed energy harvester. As for the piezoelectric laminated annular plate, multiple sets of piezoelectric ceramic sectors polarized in thickness direction are bonded to the metal substrate plate through epoxy conductive adhesive, so the metal substrate naturally becomes the common electrode of each piezoelectric ceramic sector and can be clamped to be the potential reference point for electrical analysis. The other electrode of each piezoelectric sector is the upper surface of the ceramic. The piezoelectric laminated annular plate is fixed to the central shaft through a flange coupling. The specific coaxial installation method can be seen in Figure 1 and is illustrated as follows: four sets of fastening bolts and nuts are used to fasten the flange coupling to the piezoelectric laminated annular plate via rubber washers, and then the entire system is fixed to the central shaft through four fastening screws. Thus the piezoelectric laminated annular plate is clamped on the inner ring and free on outer ring.

The analysis process of this article is illustrated in Figure 2. Firstly, based on the solid elastic theory and the basic assumption of Kirchhoff-Love plate, the differential equation for the transverse vibration of the circular thin plate is established. Secondly, the boundary conditions as well as the equivalent parameters of the laminated annular plate should be derived and substituted into the differential equation in the first step in order to learn the free vibration characteristics of a laminated

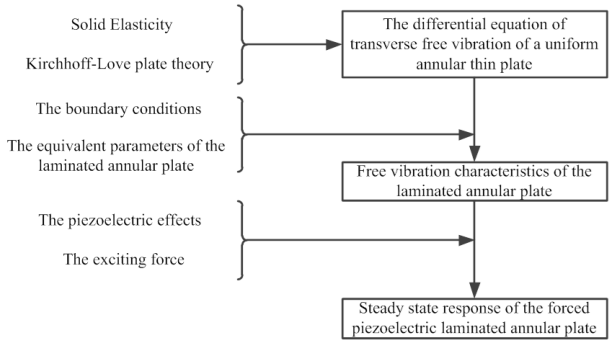


**FIGURE 2.** Analysis process of PLAPEH.

annular plate. Finally, steady state response of the piezoelectric laminated annular plate under the exciting force should be analyzed with piezoelectric effects taken into consideration.

## III. ANALYSIS OF FREE TRANSVERSE VIBRATION CHARACTERISTICS OF THE LAMINATED ANNULAR PLATE

### A. EQUIVALENT MECHANICAL PARAMETERS OF THE THIN LAMINATED PLATE

A uniform thin annular plate marked with geometric dimensions is shown in Figure 3. Based on the solid elastic theory and the Kirchhoff-Love plate theory, the differential equation for free transverse vibration of a uniform annular thin plate in polar coordinate system can be written as [25], [26]

$$D\nabla^4 w + \rho h \frac{\partial^2 w}{\partial t^2} = 0 \tag{1}$$

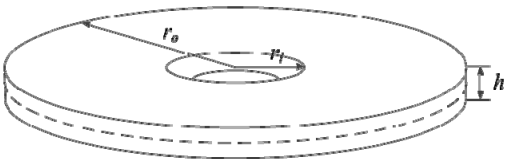


**FIGURE 3.** Schematic diagram of the thin annular plate.

where $w = w(r, \theta, t)$ is transverse deflection of the plate at position $(r, \theta)$ and time $t$, $\rho$ is the material density, $h$ is the thickness, $\nabla^4$ is Biharmonic operator, $D$ is the bending stiffness of the plate and its expression is

$$D = \frac{Yh^3}{12\left(1-\mu^2\right)} \tag{2}$$

where $Y$ and $\mu$ are the Young's modulus and Poisson's ratio of the plate, respectively.

The equivalent parameters should be derived by referring to Equation (1) in order to analyze free transverse vibration of the PLAPEH. Though the piezoelectric ceramic layer is zoned according to the vibration mode, the piezoelectric vibrator in this design can be treated as a substrate plate fully covered with the piezoelectric ceramic for free vibration analysis, because the gaps between the zones are ignorable compared to the covered zones.

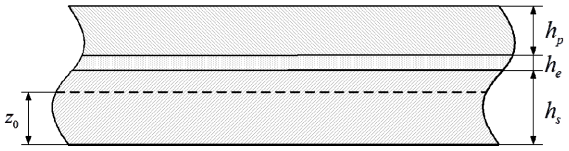


**FIGURE 4.** Thickness identification of the laminated annular plate.

I The position of the neutral plane of the laminated plate which is marked with $z_0$ in Figure 4 should be figured out first. Since the laminated thin plate is asymmetric on the z-axis, the neutral plane is not in the geometric center of the laminated plate. The thickness of each layer is marked in Figure 4, where the subscripts $s$, $e$ and $p$ denote the metal substrate layer, epoxy conductive adhesive layer and piezoelectric ceramic layer, respectively. Because the epoxy layer is extremely thin, it can be ignored (i.e. $h_e = 0$). Thus the piezoelectric ceramic is assumed to be directly bonded to the metal substrate, the strain and stress on the bonding surface are continuous. According to the bending theory of laminated plates [27]–[29], the distance from the neutral plane to the bottom of the metal substrate is

$$z_0 = \frac{1}{2}\frac{\frac{Y_s h_s^2}{1-\mu_s^2} + \frac{Y_p\left(2h_s h_p + h_p^2\right)}{1-\mu_p^2}}{\frac{Y_s h_s}{1-\mu_s^2} + \frac{Y_p h_p}{1-\mu_p^2}} \tag{3}$$

When analyzing transverse vibration of laminated plates, the coordinate origin of the z-axis is at the neutral plane. According to the definition of bending stiffness [25], the equivalent bending stiffness of the laminated annular plate is

$$D_{eq} = \frac{Y_s}{3\left(1-\mu_s^2\right)}\left[(h_s - z_0)^3 + z_0^3\right] + \frac{Y_p}{3\left(1-\mu_p^2\right)}\left[\left(h_s + h_p - z_0\right)^3 - (h_s - z_0)^3\right] \tag{4}$$

The first and second terms in the above formula are the bending stiffness of the metal substrate layer and the piezoelectric ceramic layer, respectively, which can be denoted as $D_s$ and $D_p$.

The equivalent Poisson's ratio of the laminated annular plate can be obtained by the weighted average of the Poisson's ratio of each layer where the bending stiffness is taken as the weight [30], that is

$$\mu_{eq} = \frac{D_s\mu_s + D_p\mu_p}{D_s + D_p} \tag{5}$$

Referring to Equation (1), the equivalent value of $(\rho h)$ should also be figured out as

$$(\rho h)_{eq} = \rho_s h_s + \rho_p h_p \tag{6}$$

With all the equivalent mechanical parameters listed above, the free transverse vibration characteristics of the laminated annular plate can be learned.

### B. FREE TRANSVERSE VIBRATION CHARACTERISTICS OF THE LAMINATED ANNULAR PLATE

At a certain natural frequency, each particle in the thin plate moves harmonically, so the deflection can be written as

$$w(r,\theta,t) = W(r,\theta)\, e^{i\omega t} \tag{7}$$

where $\omega$ is the circumferential natural resonance frequency of the annular thin plate, and $\omega = 2\pi f$, here $f$ is the natural resonance frequency. $W(r, \theta)$ is the corresponding vibration mode. Substituting Equation (7) to (1), we can obtain

$$D_{eq}\nabla^4 W - (\rho h)_{eq}\omega^2 W = 0 \tag{8}$$

Letting $\lambda^4 = \frac{(\rho h)_{eq}\omega^2}{D_{eq}}$, Equation (8) can be rewritten as

$$\left(\nabla^2 + \lambda^2\right)\left(\nabla^2 - \lambda^2\right) W = 0 \tag{9}$$

here $\nabla^2$ is Laplace operator.

Assuming that the solution for $W$ of the above equation can be written in the form of separate variables as [25]

$$W(r,\theta) = R(r)\,\Theta(\theta) \tag{10}$$

Substituting (10) into (9) with some arrangements, the following equation can be obtained as

$$r^2\left[\left(\frac{d^2R}{dr^2} + \frac{1}{r}\frac{dR}{dr}\right)\frac{1}{R} \pm \lambda^2\right] = -\frac{1}{\Theta}\frac{d^2\Theta}{d\theta^2} \tag{11}$$

Both sides of the above equation need to be equal to the same constant denoted by $k$, and then Equation (11) can be replaced by the following two equations as [25]

$$\frac{d^2\Theta}{d\theta^2} + k\Theta = 0 \tag{12}$$

$$r^2\left[\left(\frac{d^2R}{dr^2} + \frac{1}{r}\frac{dR}{dr}\right)\frac{1}{R} \pm \lambda^2\right] = k \tag{13}$$

General solution of Equation (12) is

$$\Theta(\theta) = A\sin\sqrt{k}\theta + B\cos\sqrt{k}\theta \tag{14}$$

Obviously, $W(r, \theta)$ has a unique value at the same location which can be expressed as

$$W(r,\theta + 2n\pi) = W(r,\theta), \quad n = 0, 1, 2, \cdots$$

Then

$$\Theta(\theta + 2n\pi) = \Theta(\theta), \quad n = 0, 1, 2, \cdots \tag{15}$$

Compare (14) with (15), the following relationship is derived as

$$k = n^2 \tag{16}$$

Then the general solution of Equation (12) can be rewritten as

$$\Theta(\theta) = A\cos n(\theta - \phi) \tag{17}$$

where $n$ is the number of radial nodal lines of a particular mode shape.

Substituting Equation (16) into (13), an $n$th order Bessel equation and modified Bessel equation can be obtained simultaneously as

$$\frac{d^2R(r)}{dr^2} + \frac{1}{r}\frac{dR(r)}{dr} + \left(\lambda^2 - \frac{n^2}{r^2}\right)R(r) = 0 \tag{18}$$

$$\frac{d^2R(r)}{dr^2} + \frac{1}{r}\frac{dR(r)}{dr} - \left(\lambda^2 + \frac{n^2}{r^2}\right)R(r) = 0 \tag{19}$$

Therefore, the general solution of Equation (13) is

$$R(r) = C_1 J_n(\lambda r) + C_2 Y_n(\lambda r) + C_3 I_n(\lambda r) + C_4 K_n(\lambda r) \tag{20}$$

where $J_n(\lambda r)$ and $K_n(\lambda r)$ are real argument Bessel functions of the first and second kind respectively, while imaginary argument Bessel functions of the first and second kind are denoted by $I_n(\lambda r)$ and $K_n(\lambda r)$.

Assuming that the mode shape is symmetrical with respect to $\theta = 0$, scilicet, $\phi = 0$ in Equation (17), then incorporating the coefficient $A$ of Equation (17) into the undetermined coefficients of Bessel functions, the general solution for $W(r, \theta)$ is rewritten as

$$W(r,\theta) = \begin{bmatrix} C_1' J_n(\lambda r) + C_2' Y_n(\lambda r) + \\ C_3' I_n(\lambda r) + C_4' K_n(\lambda r) \end{bmatrix}\cos n\theta \tag{21}$$

The laminated annular plate in this design is fixed on the inner side and free on the outer side, hence the boundary conditions can be expressed as [26]

$$\begin{cases} (w)_{r=r_i} = 0;\ \left(\dfrac{\partial w}{\partial r}\right)_{r=r_i} = 0 \\ (M_r)_{r=r_o} = 0;\ (V_r)_{r=r_o} = \left(Q_r + \dfrac{1}{r}\dfrac{\partial M_{r\theta}}{\partial\theta}\right)_{r=r_o} = 0 \end{cases} \tag{22}$$

where $M_r$ is the bending moment, $M_{r\theta}$ is the twisting moment, $Q_r$ is the transverse shear resultant, and $V_r$ is the Kirchhoff effective shear resultant on the section with a constant $r$. Substituting the expressions of the variables into the equation [24], the boundary conditions of the annular plate are

$$\begin{cases} R(r_i) = 0 \\ \left(\dfrac{dR}{dr}\right)_{r=r_i} = 0 \\ \left[\dfrac{d^2R}{dr^2} + \mu_{eq}\left(\dfrac{1}{r}\dfrac{dR}{dr} - \dfrac{n^2}{r^2}R\right)\right]_{r=r_o} = 0 \\ \left[\begin{array}{l} \dfrac{d}{dr}\left(\dfrac{d^2R}{dr^2} + \dfrac{1}{r}\dfrac{dR}{dr} - \dfrac{n^2}{r^2}R\right) \\ +\dfrac{(1-\mu_{eq})n^2}{r^2}\left(\dfrac{1}{r}R - \dfrac{dR}{dr}\right) \end{array}\right]_{r=r_o} = 0 \end{cases} \tag{23}$$

Substituting Equation (20) into the above equations, the homogeneous linear equations of the four coefficients $C_1$, $C_2$, $C_3$ and $C_4$ are obtained as

$$B\begin{bmatrix} C_1 & C_2 & C_3 & C_4 \end{bmatrix}^T = 0 \tag{24}$$

here matrix $B$ can be expressed as shown at the bottom of the next page.

The homogeneous linear equations should have non-zero solutions, so the determinant of matrix $B$ equals zero. As is known, $\lambda^4 = (\rho h)_{eq}\omega^2 / D_{eq}$, the determinant of matrix $B$ is a function of $\omega$, that is $f(\omega) = \det[B] = 0$. This equation has countless solutions as

$$\omega_{mn} = \lambda_{mn}^2 \sqrt{\frac{D_{eq}}{(\rho h)_{eq}}} \tag{25}$$

The vibration mode can be determined by substituting the natural frequency back into Equation (24), thus the natural transverse vibration characteristics of the piezoelectric laminated annular plate are obtained.

## IV. STEADY-STATE OUTPUT RESPONSE TO TRAVELLING FORCE EXCITATION OF PLAPEH

### A. DISTRIBUTED PARAMETER ELECTRO-ELASTIC MODELING OF PLAPEH

#### 1) THE FORCED VIBRATION EQUATION WITH CONSIDERATION OF PIEZOELECTRIC COUPLING

The piezoelectric vibrator in this design meets the basic assumptions of Kirchhoff plate theory and is assumed to exhibit linear electro-elastic material behavior. The linear piezoelectric constitutive equations for piezoelectric layer can be written as [26], [31], [32]

$$\begin{aligned} T_{rr} &= c_{11}^E S_{rr} + c_{12}^E S_{\theta\theta} - e_{31} E_3 \\ T_{\theta\theta} &= c_{12}^E S_{rr} + c_{11}^E S_{\theta\theta} - e_{31} E_3 \\ T_{r\theta} &= c_{66}^E S_{r\theta} \\ D_3 &= e_{31}(S_{rr} + S_{\theta\theta}) + \varepsilon_{33}^S E_3 \end{aligned} \tag{26}$$

where $T_{rr}$, $T_{\theta\theta}$ and $T_{r\theta}$ are the radial, circumferential and shear stress, while $S_{rr}$, $S_{\theta\theta}$ and $S_{r\theta}$ are the radial, circumferential and shear strain. $D_3$ and $E_3$ are electrical displacement and electric field in $z$ direction (poling direction of the piezoelectric layer). The elastic stiffness components at constant electric field $E$ are represented by $c_{11}^E$, $c_{12}^E$ and $c_{66}^E$ respectively. $\varepsilon_{33}^S$ denotes the permittivity component at constant strain $S$, and the effective piezoelectric stress constant is $e_{31}$. The electro-elasticity components in Equation (26) can be calculated by the following relations as

$$\begin{aligned} c_{11}^E &= \frac{s_{11}}{s_{11}^2 - s_{12}^2}, \quad c_{12}^E = -\frac{s_{12}}{s_{11}^2 - s_{12}^2}, \quad c_{66}^E = \frac{(c_{11}^E - c_{12}^E)}{2} \\ e_{31} &= \frac{d_{31}}{s_{11} + s_{12}}, \quad \varepsilon_{33}^S = \varepsilon_{33}^T - 2 d_{31} e_{31} \\ E_3 &= -\frac{V}{h_p}, \quad \mu_p = -\frac{s_{12}}{s_{11}}, \quad s_{11} = \frac{1}{Y_p} \end{aligned} \tag{27}$$

where $s_{11}$ and $s_{12}$ are the elastic compliance parameters, $\varepsilon_{33}^T$ is the permittivity component of the piezoelectric layer at constant stress $T$, $d_{31}$ is the piezoelectric strain constant. $\mu_p$, $Y_p$, $h_p$ and $V$ are the Poisson's ratio, Young's modulus, thickness and potential difference between the upper and lower surface of the piezoelectric layer, respectively [26], [35].

The strain components expressed in deflection is [25]

$$\begin{aligned} S_{rr} &= -z\frac{\partial^2 w}{\partial r^2}, \quad S_{\theta\theta} = -z\left(\frac{1}{r}\frac{\partial w}{\partial r} + \frac{1}{r^2}\frac{\partial^2 w}{\partial \theta^2}\right) \\ S_{r\theta} &= -z\left(-\frac{2}{r^2}\frac{\partial w}{\partial \theta} + \frac{2}{r}\frac{\partial^2 w}{\partial r \partial \theta}\right) \end{aligned} \tag{28}$$

Substituting Equation (27) and (28) into (26), the expressions of the stress components and the electric displacement of the piezoelectric layer are

$$\begin{aligned} T_{rr,p} &= -\frac{Y_p z}{1-\mu_p^2}\left[\frac{\partial^2 w}{\partial r^2} + \mu_p\left(\frac{1}{r}\frac{\partial w}{\partial r} + \frac{1}{r^2}\frac{\partial^2 w}{\partial \theta^2}\right)\right] - \frac{d_{31} Y_p}{1-\mu_p} E_3 \\ T_{\theta\theta,p} &= -\frac{Y_p z}{1-\mu_p^2}\left(\frac{1}{r}\frac{\partial w}{\partial r} + \frac{1}{r^2}\frac{\partial^2 w}{\partial \theta^2} + \mu_p\frac{\partial^2 w}{\partial r^2}\right) - \frac{d_{31} Y_p}{1-\mu_p} E_3 \\ T_{r\theta,p} &= -\frac{Y_p z}{1+\mu_p}\left(-\frac{1}{r^2}\frac{\partial w}{\partial \theta} + \frac{1}{r}\frac{\partial^2 w}{\partial r \partial \theta}\right) \\ D_3 &= -\frac{d_{31} Y_p z}{1-\mu_p}\left(\frac{\partial^2 w}{\partial r^2} + \frac{1}{r}\frac{\partial w}{\partial r} + \frac{1}{r^2}\frac{\partial^2 w}{\partial \theta^2}\right) + \varepsilon_{33}^S E_3 \end{aligned} \tag{29}$$

Similarly, the stress components of the metal substrate layer are

$$\begin{aligned} T_{rr,s} &= -\frac{Y_s z}{1-\mu_s^2}\left[\frac{\partial^2 w}{\partial r^2} + \mu_s\left(\frac{1}{r}\frac{\partial w}{\partial r} + \frac{1}{r^2}\frac{\partial^2 w}{\partial \theta^2}\right)\right] \\ T_{\theta\theta,s} &= -\frac{Y_s z}{1-\mu_s^2}\left(\frac{1}{r}\frac{\partial w}{\partial r} + \frac{1}{r^2}\frac{\partial^2 w}{\partial \theta^2} + \mu_s\frac{\partial^2 w}{\partial r^2}\right) \\ T_{r\theta,s} &= -\frac{Y_s z}{1+\mu_s}\left(-\frac{1}{r^2}\frac{\partial w}{\partial \theta} + \frac{1}{r}\frac{\partial^2 w}{\partial r \partial \theta}\right) \end{aligned} \tag{30}$$

Substituting the above stress components into the definition formulas of the moment terms [26], the bending moment and torque of piezoelectric laminated annular plate can be expressed as

$$\begin{aligned} M_{rr} &= -D_{eq}\left[\frac{\partial^2 w}{\partial r^2} + \mu_{eq}\left(\frac{1}{r}\frac{\partial w}{\partial r} + \frac{1}{r^2}\frac{\partial^2 w}{\partial \theta^2}\right)\right] - KE_3 \\ M_{\theta\theta} &= -D_{eq}\left(\frac{1}{r}\frac{\partial w}{\partial r} + \frac{1}{r^2}\frac{\partial^2 w}{\partial \theta^2} + \mu_{eq}\frac{\partial^2 w}{\partial r^2}\right) - KE_3 \\ M_{r\theta} &= -D_{eq}(1-\mu_{eq})\left(-\frac{1}{r^2}\frac{\partial w}{\partial \theta} + \frac{1}{r}\frac{\partial^2 w}{\partial r \partial \theta}\right) \end{aligned} \tag{31}$$

$$B = \begin{pmatrix} J_n(\lambda r)|_{r=r_i} & Y_n(\lambda r)|_{r=r_i} & I_n(\lambda r)|_{r=r_i} & K_n(\lambda r)|_{r=r_i} \\ \frac{\partial}{\partial r}J_n(\lambda r)\Big|_{r=r_i} & \frac{\partial}{\partial r}Y_n(\lambda r)\Big|_{r=r_i} & \frac{\partial}{\partial r}I_n(\lambda r)\Big|_{r=r_i} & \frac{\partial}{\partial r}K_n(\lambda r)\Big|_{r=r_i} \\ M_r(J_n(\lambda r))|_{r=r_o} & M_r(Y_n(\lambda r))|_{r=r_o} & M_r(I_n(\lambda r))|_{r=r_o} & M_r(K_n(\lambda r))|_{r=r_o} \\ V_r(J_n(\lambda r))|_{r=r_o} & V_r(Y_n(\lambda r))|_{r=r_o} & V_r(I_n(\lambda r))|_{r=r_o} & V_r(K_n(\lambda r))|_{r=r_o} \end{pmatrix}$$

where $K$ is the piezoelectric moment constant which can be calculated as

$$K = \int_{h_s-z_0}^{h_p+h_s-z_0} \frac{d_{31}Y_p}{1-\mu_p} z dz = \frac{d_{31}Y_p}{1-\mu_p} \frac{z^2}{2}\Big|_{h_s-z_0}^{h_p+h_s-z_0} = \frac{d_{31}Y_p h_p \left(h_p+2h_s-2z_0\right)}{2\left(1-\mu_p\right)} = \frac{d_{31}Y_p h_p h_{pc}}{\left(1-\mu_p\right)} = e_{31}h_p h_{pc} \tag{32}$$

where $h_{pc}$ represents the distance from geometric mid-plane of the piezoelectric layer to the neutral plane of the laminated plate, which is

$$h_{pc} = \frac{h_p + 2h_s - 2z_0}{2}$$

The transverse shear forces of the piezoelectric laminated annular plate is [26]

$$\begin{aligned} Q_r &= \frac{\partial M_{rr}}{\partial r} + \frac{1}{r}\left(M_{rr} - M_{\theta\theta}\right) + \frac{1}{r}\frac{\partial M_{r\theta}}{\partial \theta} \\ Q_\theta &= \frac{\partial M_{r\theta}}{\partial r} + \frac{1}{r}\frac{\partial M_{\theta\theta}}{\partial \theta} + \frac{2}{r}M_{r\theta} \end{aligned} \tag{33}$$

As is shown in Figure 1, the piezoelectric ceramic layer is zoned according to the vibration mode and there is a gap at a fixed angle between each zone. The electric field only exists in piezoelectric ceramics, so it can be expressed as

$$E_3 = E_3(t)\,\Phi(r,\theta) \tag{34}$$

where

$$\Phi(r,\theta) = \Gamma(r)\,\Psi(\theta) \tag{35}$$

and

$$\begin{aligned} \Gamma(r) &= H\left(r - r_i - r_{gi}\right) - H\left(r - r_o + r_{go}\right) \\ \Psi(\theta) &= \sum_{k=1}^{N}\left[H\left(\theta - k\theta_s + \theta_s\right) - H\left(\theta - k\theta_s + \theta_g\right)\right] \end{aligned} \tag{36}$$

where $H$ is the Heaviside step function, $\theta_s$ is the angular of each zone with the gap included, $\theta_g$ is the angular of the gap between each zone, $N$ is the number of the zones, so $\theta_s = 2\pi/N$. Considering that the piezoelectric layer and the electrode will not be completely laid to the inner and outer boundaries of the substrate layer, so there are gaps $r_{gi}$ and $r_{go}$ in reality. But the gaps are ignorable (i.e. $r_{gi} = r_{go} = 0$) in theoretical analysis. So Equation (33) can be rewritten as

$$\begin{aligned} Q_r &= -D_{eq}\frac{\partial}{\partial r}\nabla^2 w - KE_3\frac{\partial \Phi(r,\theta)}{\partial r} \\ Q_\theta &= -D_{eq}\frac{1}{r}\frac{\partial}{\partial \theta}\nabla^2 w - KE_3\frac{1}{r}\frac{\partial \Phi(r,\theta)}{\partial \theta} \end{aligned} \tag{37}$$

The differential equation for forced vibration of piezoelectric laminated annular plate under transverse excitation force is

$$-\frac{\partial Q_r}{\partial r} - \frac{Q_r}{r} - \frac{1}{r}\frac{\partial Q_\theta}{\partial \theta} + (\rho h)_{eq}\frac{\partial^2 w}{\partial t^2} = q(r,\theta,t) \tag{38}$$

where $q(r,\theta,t)$ is the transverse force term. Substituting Equation (37) into (38), defining the electric field in terms of the electrical potential difference as $E_3(t) = -V(t)/h_p$, the forced vibration equation with respect to system damping $\beta$ of the PLAPEH is

$$D_{eq}\nabla^4 w + \beta\frac{\partial w}{\partial t} - \frac{K}{h_p}\nabla^2\Phi V(t) + (\rho h)_{eq}\frac{\partial^2 w}{\partial t^2} = q(r,\theta,t) \tag{39}$$

where

$$\begin{aligned} \nabla^2\Phi &= \frac{\partial^2\Phi(r,\theta)}{\partial r^2} + \frac{1}{r}\frac{\partial\Phi(r,\theta)}{\partial r} + \frac{1}{r^2}\frac{\partial^2\Phi(r,\theta)}{\partial\theta^2} \\ &= \Psi(\theta)\left[\frac{d^2\Gamma(r)}{dr^2} + \frac{1}{r}\frac{d\Gamma(r)}{dr}\right] + \frac{1}{r^2}\Gamma(r)\frac{d^2\Psi(\theta)}{d\theta^2} \end{aligned} \tag{40}$$

### 2) THE ELECTRICAL CIRCUIT EQUATION

The electric displacement in Equation (29) is

$$D_3 = -\frac{d_{31}Y_p z}{1-\mu_p}\nabla^2 w + \varepsilon_{33}^S E_3 \tag{41}$$

Integrating the terms of Equation (41) along the z-axis in the piezoelectric layer, then the electric displacement is

$$D_3 = -e_{31}h_{pc}\nabla^2 w - \varepsilon_{33}^S\frac{V(t)}{h_p} \tag{42}$$

A resistive load $R_l$ is connected to a piezoelectric sector, the current flowing to the resistive load can be derived as [21]

$$\frac{d}{dt}\int_A \mathbf{D}\cdot\mathbf{n}dA = \frac{V(t)}{R_l} \tag{43}$$

where $\mathbf{n}$ is the unit vector outward from the electrode surface of the piezoelectric ceramic sector while $\mathbf{D}$ is the electric displacement vector. The inner product of $\mathbf{n}$ and $\mathbf{D}$ yields the electric displacement term $D_3$ in Equation (42). The integral is over surface of the electrode and its area is denoted by $A$ [21]. The differential equation of the coupled electrical circuit is derived by substituting Equation (42) into Equation (43) as

$$C_p\frac{dV(t)}{dt} + \frac{V(t)}{R_l} + e_{31}h_{pc}\int_0^{\theta_s-\theta_g}\int_{r_i}^{r_o}\frac{d}{dt}\left(\frac{\partial^2 w}{\partial r^2} + \frac{1}{r}\frac{\partial w}{\partial r} + \frac{1}{r^2}\frac{\partial^2 w}{\partial\theta^2}\right)drd\theta = 0 \tag{44}$$

where $C_p$ is the equivalent capacitance which can be calculated as

$$C_p = \frac{\left(\theta_s-\theta_g\right)\left(r_o^2 - r_i^2\right)\varepsilon_{33}^S}{2h_p} \tag{45}$$

Therefore, the distributed parameter electro-elastic model of PLAPEH can be represented by Equation (39) and (44).

### B. STEADY-STATE RESPONSE TO THE EXCITING FORCE

The distributed parameter electro-elastic model equation can be solved by modal expansion [33] as

$$w(r,\theta,t)=\sum_{m=0}^{\infty}\sum_{n=1}^{\infty}W_{mn}(r,\theta)\,\eta_{mn}(t) \tag{46}$$

where $W_{mn}(r,\theta)$ is the mode shape, $\eta_{mn}(t)$ is the time response in modal coordinate for the $mn$th vibration mode. Substituting Equation (46) into Equation (39) yields

$$\sum_{m=0}^{\infty}\sum_{n=1}^{\infty}\begin{pmatrix}D_{eq}\nabla^4 W_{mn}(r,\theta)\,\eta_{mn}(t)+\beta W_{mn}(r,\theta)\,\dot{\eta}_{mn}(t)\\+(\rho h)_{eq}\,W_{mn}(r,\theta)\,\ddot{\eta}_{mn}(t)\end{pmatrix}-\frac{K}{h_p}\nabla^2\Phi V(t)=q(r,\theta,t) \tag{47}$$

here

$$q(r,\theta,t)=\frac{F_0}{r}\delta\left(r-r^*\right)\delta\left(\theta-\theta^*\right) \tag{48}$$

where $\delta(r-r^*)$ and $\delta(\theta-\theta^*)$ are Dirac deltas which locate the transverse exciting force at $(r^*,\theta^*)$. The angular velocity of the travelling force is constant which is denoted by $\Omega$, so $\theta^*=\Omega t$ in Equation (48). Substituting Equation (8) into Equation (47) and making use of orthogonality of modes by multiplying Equation (47) by $W_{pq}(r,\theta)$, then integrating over the domain of the annular plate, yields

$$\begin{aligned}&\sum_{m=0}^{\infty}\sum_{n=1}^{\infty}\left((\rho h)_{eq}\,\ddot{\eta}_{mn}(t)+\beta\dot{\eta}_{mn}(t)+(\rho h)_{eq}\,\omega_{mn}^2\eta_{mn}(t)\right)\\&\quad\times\int_0^{2\pi}\int_{r_i}^{r_o}W_{mn}(r,\theta)\,W_{pq}(r,\theta)\,r\mathrm{d}r\mathrm{d}\theta\\&\quad-\frac{K}{h_p}V(t)\int_0^{2\pi}\int_{r_i}^{r_o}\nabla^2\Phi(r,\theta)\,W_{pq}(r,\theta)\,r\mathrm{d}r\mathrm{d}\theta\\&=\int_0^{2\pi}\int_{r_i}^{r_o}q_3(r,\theta,t)\,W_{pq}(r,\theta)\,r\mathrm{d}r\mathrm{d}\theta\end{aligned} \tag{49}$$

Defining modal orthogonality as

$$\iint W_{mn}(r,\theta)\,W_{pq}(r,\theta)\,r\mathrm{d}r\mathrm{d}\theta=\delta_{mp}\delta_{nq}N_{mn} \tag{50}$$

where $\delta_{mp}$ and $\delta_{nq}$ are the Kronecker delta function which means $\delta_{mp}=1$ when $m=p$, while $\delta_{mp}=0$ when $m\neq p$, same as $\delta_{nq}$. $N_{mn}$ in Equation (50) can be calculated as $N_{mn}=\iint W_{mn}^2(r,\theta)\,r\mathrm{d}r\mathrm{d}\theta$.

The energy harvester is designed to operate at its lowest critical speed which occurs at the first radial mode (i.e. m=0). Exploring orthogonality in Equation (49), defining modal damping as $\xi_n=\frac{\beta}{2(\rho h)_{eq}\omega_n}$, and replacing $W_{mn}$ and $\eta_{mn}$ with $W_n$ and $\eta_n$, we can obatain

$$\ddot{\eta}_n(t)+2\xi_n\omega_n\dot{\eta}_n(t)+\omega_n^2\eta_n(t)=G_nV(t)+T_nf(t) \tag{51}$$

here, $\omega_n$ is the undamped natural frequency for the $n$th vibration mode and

$$T_n=\frac{F_0R_n(r^*)}{N_n(\rho h)_{eq}} \tag{52}$$

$$f(t)=\begin{cases}\cos n\Omega t\\ \sin n\Omega t\end{cases} \tag{53}$$

$$G_n=\frac{K}{N_nh_p(\rho h)_{eq}}\int_0^{2\pi}\int_{r_i}^{r_o}\nabla^2\Phi(r,\theta)\,W_n(r,\theta)\,r\mathrm{d}r\mathrm{d}\theta \tag{54}$$

where $G_n$ represents the modal electromechanical coupling term and $N_n$ can be calculated as

$$N_n=\int_0^{2\pi}\Theta_n^2(\theta)\,\mathrm{d}\theta\int_{r_i}^{r_o}R_n^2(r)\,r\mathrm{d}r$$

Substituting Equation (5), (40) and boundary conditions into Equation (54) to expand the integral in the equation, then $G_n$ can be recast as

$$\begin{aligned}G_n=&\frac{K\int_0^{2\pi}\Psi(\theta)\,\Theta_n(\theta)\,\mathrm{d}\theta}{N_nh_p\left(\rho_sh_s+\rho_ph_p+\rho_eh_e\right)}\\&\times\left(r_o\frac{\mathrm{d}R_n(r_o)}{\mathrm{d}r_o}-n^2\int_{r_i}^{r_o}\frac{R_n(r)}{r}\mathrm{d}r\right)\end{aligned} \tag{55}$$

Substituting Equation (46) into Equation (44), we can obtain the electrical circuit equation in modal coordinates as

$$\begin{aligned}&C_p\frac{dV(t)}{dt}+\frac{V(t)}{R_l}\\&\quad+\sum_{n=1}^{\infty}e_{31}h_{pc}\frac{d\eta_n(t)}{dt}\int_0^{\theta_s-\theta_g}\int_{r_i}^{r_o}\nabla^2W_n(r,\theta)\,dr\mathrm{d}\theta=0\end{aligned} \tag{56}$$

where

$$\begin{aligned}&\int_0^{\theta_s-\theta_g}\int_{r_i}^{r_o}\nabla^2W_n(r,\theta)\,r\mathrm{d}r\mathrm{d}\theta\\&=\int_0^{\theta_s-\theta_g}\Theta_n(\theta)\,\mathrm{d}\theta\left(r\frac{\mathrm{d}R_n(r)}{\mathrm{d}r}\middle|_{r_i}^{r_o}-n^2\int_{r_i}^{r_o}\frac{R_n(r)}{r}\mathrm{d}r\right)\end{aligned} \tag{57}$$

Dividing each term in Equation (56) by $C_p$, we can obtain

$$\frac{dV(t)}{dt}+\frac{V(t)}{R_lC_p}=-\sum_{n=1}^{\infty}H_n\frac{d\eta_n(t)}{dt} \tag{58}$$

where

$$\begin{aligned}H_n=&\frac{e_{31}h_{pc}}{C_p}\int_0^{\theta_s-\theta_g}\int_{r_i}^{r_o}\nabla^2W_n(r,\theta)\,r\mathrm{d}r\mathrm{d}\theta\\=&\frac{e_{31}h_{pc}}{C_p}\int_0^{\theta_s-\theta_g}\Theta_n(\theta)\,\mathrm{d}\theta\left(r\frac{\mathrm{d}R_n(r)}{\mathrm{d}r}\middle|_{r_i}^{r_o}\right.\\&\left.-n^2\int_{r_i}^{r_o}\frac{R_n(r)}{r}\mathrm{d}r\right)\end{aligned} \tag{59}$$

The forced vibration equation and electric circuit equation of the PLAPEH in modal coordinates are represented by Equation (51) and (58) respectively. For vibration under the excitation of a rotating point-wise force with an angular velocity of $\Omega$, the modal participation factor of the piezoelectric laminated annular plate in modal coordinates and the

steady-state response of the voltage across the resistive load can be expressed as

$$\eta_n(t) = \kappa_n e^{j\omega t}, \quad V(t) = V_s e^{j\omega t} \tag{60}$$

where $\omega = n\Omega$.

Substituting Equation (60) into Equation (51) and (58), yields

$$\left(\omega_n^2 - \omega^2 + 2j\xi_n\omega_n\omega\right)\kappa_n = G_n V_s + T_n \tag{61}$$

$$\left(j\omega + \frac{1}{R_l C_p}\right) V_s = -j\omega \sum_{n=1}^{\infty} \kappa_n H_n \tag{62}$$

From Equation (61), one can obtain

$$\kappa_n = \frac{G_n V_s + T_n}{\left(\omega_n^2 - \omega^2 + 2j\xi_n\omega_n\omega\right)} \tag{63}$$

Substituting Equation (63) into Equation (62), the steady-state voltage amplitude across the resistive load is

$$V_s = -\frac{j\omega \sum_{n=1}^{\infty} \frac{T_n H_n}{\omega_n^2 - \omega^2 + j2\xi_n\omega_n\omega}}{j\omega + \frac{1}{R_l C_p} + j\omega \sum_{n=1}^{\infty} \frac{G_n H_n}{\omega_n^2 - \omega^2 + j2\xi_n\omega_n\omega}} \tag{64}$$

The power output from a single piezoelectric ceramic to the resistive load can be calculated as

$$P_l = \frac{V_s^2}{2R_l} \tag{65}$$

Then, when the vibration mode is (0, $n$), the total output power of $N$ ($N = 2n$) piezoelectric sectors is

$$P_o = N\frac{V_s^2}{2R_l} \tag{66}$$

The maximum power can be obtained by matching the impedance of the load resistance to the source impedance of the energy harvester, and the optimum load resistance can be solved by

$$\frac{\partial P_o}{\partial R_l} = 0 \rightarrow R_l^{opt} = \frac{1}{\omega C_p} \tag{67}$$

Substituting Equation (64) back into Equation (61), one can obtain

$$\kappa_n = \left( T_n - G_n \frac{j\omega \sum_{n=1}^{\infty} \frac{T_n H_n}{\omega_n^2 - \omega^2 + j2\xi_n\omega_n\omega}}{j\omega + \frac{1}{R_l C_p} + j\omega \sum_{n=1}^{\infty} \frac{G_n H_n}{\omega_n^2 - \omega^2 + j2\xi_n\omega_n\omega}} \right) \times \frac{1}{\omega_n^2 - \omega^2 + j2\xi_n\omega_n\omega} \tag{68}$$

Then, the transverse deflection of the piezoelectric laminated annular plate is

$$w(r,\theta,t) = \sum_{n=1}^{\infty} W_n(r,\theta)\,\eta_n(t) = \sum_{n=1}^{\infty} R_n(r)\,\Theta_n(\theta)\,\kappa_n e^{j\omega t} \tag{69}$$

**TABLE 1. Geometric and material parameters.**

| Parameters | Substrate | PZT |
|---|---|---|
| Material | Steel | 5A |
| Yong's modulus, $Y$ (GPa) | 200 | 61 |
| Density, ρ (kg/m3) | 7800 | 7700 |
| Piezoelectric strain constant, $d_{31}$ ( pm/V) | - | -171 |
| Permittivity, $\varepsilon_{33}^{T}$ ( nF/m) | - | 15.05 |
| Poisson's ratio, $\mu$ | 0.33 | 0.31 |
| Thickness, $h$ (mm) | 0.5 | 0.5 |
| Inner radius, $r_i$ (mm) | 10 | |
| Outer radius, $r_o$ （mm） | 70 | |
| Exciting force, $F_0$ (N) | 0.5 | |
| Damping ratio， $\xi_n$ | 0.012 | |
| Radial position of force, $r^*$ （mm） | $0.95\times r_o$ | |

## V. RESULTS AND DISCUSSION

In order to validate the analytical modeling established in this article, finite element analysis (FEA) is done by the commercial software COMSOL with the geometric dimensions and material characters listed in Table 1. COMSOL is quite suitable for numerical analysis for piezoelectric energy harvesting devices because a multi-physics coupling platform is provided in it. Piezoelectric Devices, Solid Mechanics and Electrical Circuit interfaces are used in our analysis. Piezoelectric sectors and the steel substrate plate are united by using form union in Geometry domain. In Solid Mechanics domain, fixed constrain is applied to the inner boundary (i.e. $r = r_i$) of the laminated plate, and the remaining boundaries are free. The build-in Electrostatic can be used to set the electrical boundary conditions of the piezoelectric layer. The bottom electrodes of the piezoelectric ceramics are clamped to zero by applying ground boundary to them, and the upper surface of each piezoelectric sector is clamped to be the other electrode by setting it as a circuit terminal with no initial charge. Four resistive loads with the same value are connected to the ground and each circuit terminal separately. Eigen frequency study is performed to analyze free transverse vibration of the piezoelectric laminated plate, and a short-circuit condition is applied by setting the resistive load to be 1 Ω. Frequency domain studies are performed to evaluate the output responses of the PLAPEH subjected to the travelling point-wise force.

**TABLE 2. Natural frequency for different circumferential modes when m = 0.**

| n | 0 | 1 | 2 | 3 | 4 | 5 |
|---|---|---|---|---|---|---|
| Analytical (Hz) | 165.81 | 144.93 | 210.54 | 445.44 | 779.83 | 119.93 |
| FEA (Hz) | 171.42 | 149.17 | 210.42 | 443.96 | 778.64 | 1196.70 |
| Error (%) | 3.27 | 2.84 | 0.05 | 0.33 | 0.16 | 0.02 |

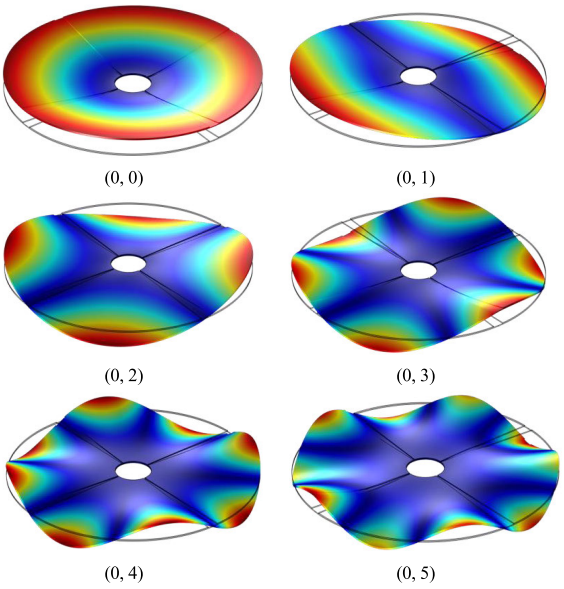


**FIGURE 5.** Vibration mode shapes for different circumferential modes when m = 0.

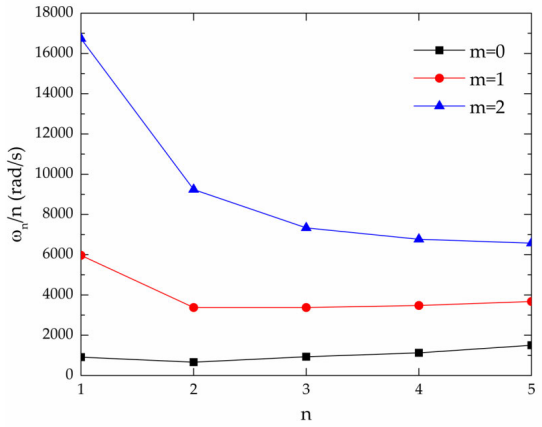


**FIGURE 6.** Rotating speeds of the travelling force for different vibration modes.

The vibration modes and the corresponding frequency of the piezoelectric laminated annular plate are shown in Table 2 where the FEA results are also included. The corresponding vibration mode shapes can be seen in Figure 5. The comparison between analytical and FEA results shows that the theoretical analysis method proposed in this article offers an effective way to evaluate the free transverse vibration characteristics of the PLAPEH.

Mode (0, 2) is chosen as the target mode because the rotating speed of the travelling exciting force is lowest in this mode as is illustrated in Figure 6 which is desirable for application. When the equivalent angular velocity of the rotating force is close to the natural frequency of a certain vibration mode, the output responses could be supposed to be only affected by the dominant vibration mode and several nearby modes which indicates the upper boundary of the sum term in Equation (64) and (68) is a finite number in this approximation [26], [31]. The piezoelectric layer is composed of

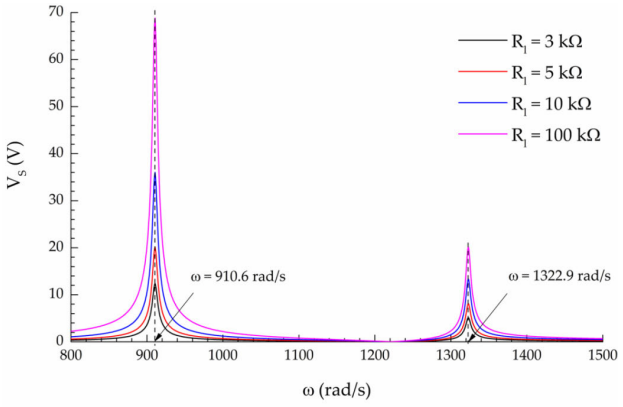


**FIGURE 7.** Output voltage amplitude *versus* $\omega$ ranging from 800 to 1500 rad/s with different $R_l$.

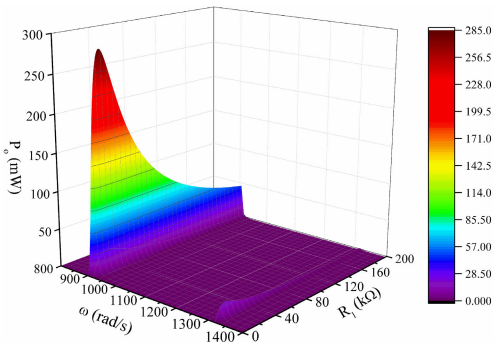


**FIGURE 8.** Output power with different $\omega$ and $R_l$.

four separate sectors with proper electrodes arrangement according to the mode shape, and there is an angular gap of 10 degrees between each sector. Charge cancellation can be averted both in radial and circumferential direction by using this configuration, and the analytical model proposed in this article can also be implemented for the performance prediction of the PLAPEH working at mode (0, 1).

More information can be acquired by expanding the observation range of the equivalent angular velocity. And the relationship between the steady-state voltage response of the forced PLAPEH and the equivalent angular velocity of the exciting force with different resistive loads connected is shown in Figure 7. With different resistive loads connected, the amplitude of the output voltage have two peeks at the same equivalent angular velocities of 910.6 rad/s and 1322.9 rad/s over the expanded angular velocity ranging from 800 to 1500 rad/s. The peak voltage at 910.6 rad/s which is the angular velocity of mode (0, 1) is much higher than the value of the target mode (0, 2) with the same resistive load connected.

The output power of the forced PLAPEH changes with the equivalent angular velocity $\omega$ and resistive load $R_l$. And the relationships are illustrated in Figure 8. The output power of mode (0, 1) is much higher than that of mode (0, 2).

In order to know more details about the performance of proposed energy harvester, we explore the output power of

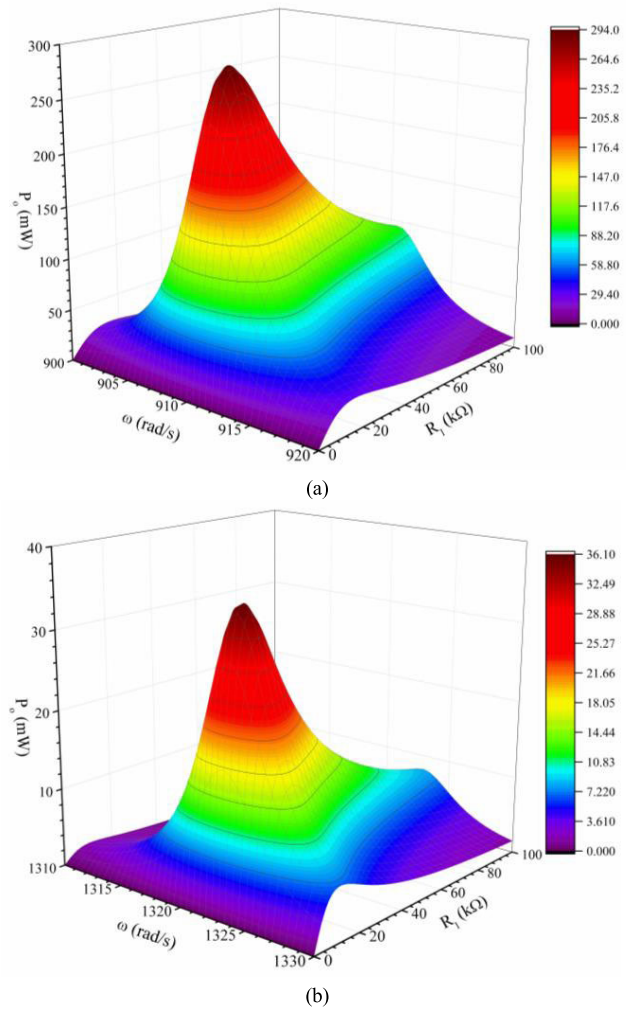


**FIGURE 9.** Output power versus equivalent angular velocity of the exciting force with different load resistance at (a) mode (0, 1) and (b) mode (0, 2).

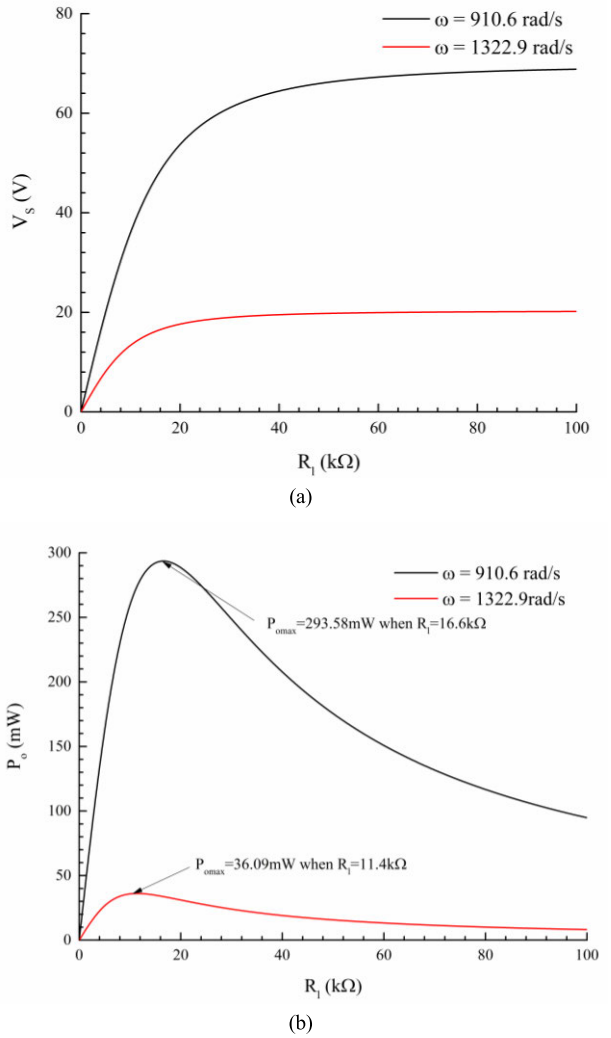


**FIGURE 10.** Output voltage amplitude (a) and output power (b) *versus* load resistance when $\omega = 910.6$ rad/s and 1322.9 rad/s.

PLAPEH under the exciting force with equivalent angular velocity ranging from 900 to 920 rad/s and 1310 to 1330 rad/s when different load resistances are connected. And the results are illustrated in Figure 9 (a) and (b). The maximum power for mode (0, 1) can reach up to more than 290 mW while that for mode (0, 2) is more than 36 mW. We also find that, the peak output voltage amplitude and output power can be achieved at the point when the equivalent angular velocity of the exciting force is 910.6 rad/s and 1322.9 rad/s respectively.

The output performances at the two angular velocities mentioned above are shown in Figure 10 (a) and (b). The amplitude of the output voltage increases rapidly with the resistive load when the value of the resistor is small, after that the growth rate reduces as the resistive load increases and gradually comes to a standstill. For mode (0, 2), a maximum power of 36.09 mW can be achieved when the optimum resistive load of 11.4 kΩ is connected. While a maximum power of 293.58 mW can be achieved when the optimum resistive load of 16.6 kΩ is connected at mode (0, 1). Actually, the optimum resistive load here is 1.45 times of that value when the equivalent rotating angular velocity is 1322.9 rad/s, and this result coincides with the expression of the optimum resistive load in Equation (67).

## VI. CONCLUSION

A piezoelectric laminated annular plate for rotary energy harvesting is creatively proposed in this article, and this structure is based on the standing wave vibration of the plate. The analytical modeling is established to predict the output performance of the proposed energy harvester. Compared with FEA methods, the theoretical analysis method proposed in this article is more effective and reliable, and can reduce the computation cost. Mode (0, 2) is chosen as the target mode shape and the corresponding layout of the piezoelectric layer with consideration of avoiding charge cancellation for this mode shape is also introduced in detail in this article. The analytical results show that the output power from a few to tens of milliwatts can be achieved with the optimal resistance connected to the energy harvester. Comparing with the target

mode, we find that the output features of mode (0, 1) are much better. So more detailed research should be conducted to determine which mode shape is much better in a specific application. Only mode shape is taken into consideration to avert charge cancellation in this article. However, more factors which can affect the performance of PLAPEH should be considered to optimize the layout of the piezoelectric ceramics in the near future.

## REFERENCES

[1] H. Elahi, M. Eugeni, and P. Gaudenzi, "A review on mechanisms for piezoelectric-based energy harvesters," *Energies*, vol. 11, no. 7, p. 1850, Jul. 2018.
[2] M. Shirvanimoghaddam, K. Shirvanimoghaddam, M. M. Abolhasani, M. Farhangi, V. Z. Barsari, H. Liu, M. Dohler, and M. Naebe, "Towards a green and self-powered Internet of Things using piezoelectric energy harvesting," *IEEE Access*, vol. 7, pp. 94533–94556, Jul. 2019.
[3] T. H. Ng and W. H. Liao, "Feasibility study of a self-powered piezoelectric sensor," *Proc. SPIE*, vol. 5389, pp. 377–388, Jul. 2004.
[4] J. M. Dietl and E. Garcia, "Beam shape optimization for power harvesting," *J. Intell. Mater. Syst. Struct.*, vol. 21, no. 6, pp. 633–646, Mar. 2010.
[5] A. Erturk, J. Hoffmann, and D. J. Inman, "A piezomagnetoelastic structure for broadband vibration energy harvesting," *Appl. Phys. Lett.*, vol. 94, no. 25, Jun. 2009, Art. no. 254102.
[6] Z. Yang and J. Yang, "Connected vibrating piezoelectric bimorph beams as a wide-band piezoelectric power harvester," *J. Intell. Mater. Syst. Struct.*, vol. 20, no. 5, pp. 569–574, Mar. 2009.
[7] A. Erturk, J. M. Renno, and D. J. Inman, "Modeling of piezoelectric energy harvesting from an L-shaped beam-mass structure with an application to UAVs," *J. Intell. Mater. Syst. Struct.*, vol. 20, no. 5, pp. 529–544, Mar. 2009.
[8] M. Ferrari, V. Ferrari, M. Guizzetti, B. Andu, S. Baglio, and C. Trigona, "Improved energy harvesting from wideband vibrations by nonlinear piezoelectric converters," *Sens. Actuators A, Phys.*, vol. 162, no. 2, pp. 425–431, Aug. 2010.
[9] M. A. Karami and D. J. Inman, "Analytical modeling and experimental verification of the vibrations of the zigzag microstructure for energy harvesting," *J. Vibrat. Acoust.*, vol. 133, no. 1, Feb. 2011, Art. no. 011002.
[10] H. W. Kim, A. Batra, S. Priya, K. Uchino, D. Markley, R. E. Newnham, and H. F. Hofmann, "Energy harvesting using a piezoelectric 'cymbal' transducer in dynamic environment," *Jpn. J. Appl. Phys.*, vol. 43, no. 9, pp. 6178–6183, 2004.
[11] A. Moure, M. A. I. Rodríguez, S. H. Rueda, A. Gonzalo, F. Rubio-Marcos, D. U. Cuadros, A. Pérez-Lepe, and J. F. Fernández, "Feasible integration in asphalt of piezoelectric cymbals for vibration energy harvesting," *Energy Convers. Manage.*, vol. 112, pp. 246–253, Mar. 2016.
[12] M. Leinonen, J. Palosaari, J. Juuti, and H. Jantunen, "Combined electrical and electromechanical simulations of a piezoelectric cymbal harvester for energy harvesting from walking," *J. Intell. Mater. Syst. Struct.*, vol. 25, no. 4, pp. 391–400, Aug. 2013.
[13] X. Li, M. Guo, and S. Dong, "A flex-compressive-mode piezoelectric transducer for mechanical vibration/strain energy harvesting," *IEEE Trans. Ultrason., Ferroelectr., Freq. Control*, vol. 58, no. 4, pp. 698–703, Apr. 2011.
[14] P. H. Goh, M.-J. Li, and N.-T. Tsou, "The design and analysis for low-frequency piezoelectric cymbal transducers," *Ceram. Int.*, vol. 43, pp. S49–S54, Aug. 2017.
[15] B. S. Lee, S. C. Lin, and W. J. Wu, "Comparison of the piezoelectric MEMS generators with interdigital electrodes and laminated electrodes," *Proc. SPIE*, vol. 6933, pp. 232–241, Apr. 2008.
[16] N. Rezaei-Hosseinabadi, A. Tabesh, R. Dehghani, and A. Aghili, "An efficient piezoelectric windmill topology for energy harvesting from low-speed air flows," *IEEE Trans. Ind. Electron.*, vol. 62, no. 6, pp. 3576–3583, Jun. 2015.
[17] M. A. Karami, J. R. Farmer, and D. J. Inman, "Parametrically excited nonlinear piezoelectric compact wind turbine," *Renew. Energy*, vol. 50, pp. 977–987, Feb. 2013.
[18] H. J. Jung, Y. Song, S. K. Hong, C. H. Yang, S. J. Hwang, S. Y. Jeong, and T. H. Sung, "Design and optimization of piezoelectric impact-based micro wind energy harvester for wireless sensor network," *Sens. Actuators A, Phys.*, vol. 222, pp. 314–321, Feb. 2015.
[19] Y. Kuang and M. Zhu, "Characterisation of a knee-joint energy harvester powering a wireless communication sensing node," *Smart Mater. Struct.*, vol. 25, no. 5, Apr. 2016, Art. no. 055013.
[20] Y. Wang, Z. Yang, P. Li, D. Cao, W. Huang, and D. J. Inman, "Energy harvesting for jet engine monitoring," *Nano Energy*, vol. 75, Sep. 2020, Art. no. 104853.
[21] U. Aridogan, I. Basdogan, and A. Erturk, "Analytical modeling and experimental validation of a structurally integrated piezoelectric energy harvester on a thin plate," *Smart Mater. Struct.*, vol. 23, no. 4, Mar. 2014, Art. no. 045039.
[22] U. Aridogan, I. Basdogan, and A. Erturk, "Multiple patch–based broadband piezoelectric energy harvesting on plate-based structures," *J. Intell. Mater. Syst. Struct.*, vol. 25, no. 14, pp. 1664–1680, Sep. 2014.
[23] R. Ahmed and S. Banerjee, "Predictive electromechanical model for energy scavengers using patterned piezoelectric layers," *J. Eng. Mech.*, vol. 141, no. 2, Feb. 2015, Art. no. 04014113.
[24] J. Kan, J. Fu, S. Wang, Z. Zhang, S. Chen, and C. Yang, "Study on a piezo-disk energy harvester excited by rotary magnets," *Energy*, vol. 122, pp. 62–69, Mar. 2017.
[25] Z. Xu, *Theory of Elasticity*, 4th ed. Beijing, China: Higher Education Press, 2013, pp. 1-8–1-220.
[26] J. Wang, W. Su, C. Wang, *Piezoelectric Vibration Theory and Application*. Beijing, China: Science Press, 2011, pp. 5–14, 27–30, and 68–85.
[27] T. Peng, J. Kan, Z. Yang, and G. Cheng, "Numerical simulation and experiments on bending vibration characteristics of circular piezoelectric vibrator," (in Chinese), *China Mech. Eng.*, vol. 20, no. 16, pp. 1987–1991, Aug. 2009.
[28] W. Soedel, *Vibrations of Shells and Plates*, 3rd ed. Boca Raton, FL, USA: CRC Press, 2004.
[29] P. R. Heyliger and G. Ramirez, "Free vibration of laminated circular piezoelectric plates and discs," *J. Sound Vibrat.*, vol. 229, no. 4, pp. 935–956, Jan. 2000.
[30] M. Brissaud, "Theoretical modelling of non-symmetric circular piezoelectric bimorphs," *J. Micromech. Microeng.*, vol. 16, no. 5, pp. 875–885, Mar. 2006.
[31] A. Erturk and D. J. Inman, *Piezoelectric Energy Harvesting*. New York, NY, USA: Wiley, 2011, pp. 1–14.
[32] S. Priya and D. J. Inman, *Energy Harvesting Technologies*. Berlin, Germany: Springer, 2009, pp. 129–159.
[33] S. S. Rao, *Vibration of Continuous Systems*. Miami, FL, USA: Wiley, 2007.
[34] T. Guo, Z. Xu, L. Jin, and M. Hu, "Optimized structure design of a bridge-like piezoelectric energy harvester based on finite element analysis," in *Proc. 20th Int. Conf. Electr. Mach. Syst. (ICEMS)*, Sydney, NSW, Australia, Aug. 2017, pp. 1–5.
[35] N. Elvin and A. Erturk, *Advances in Energy Harvesting Methods*. New York, NY, USA: Springer, 2013.
[36] S. Kim, W. W. Clark, and Q.-M. Wang, "Piezoelectric energy harvesting with a clamped circular plate: Analysis," *J. Intell. Mater. Syst. Struct.*, vol. 16, no. 10, pp. 847–854, Oct. 2005.
[37] A. Erturk, P. A. Tarazaga, J. R. Farmer, and D. J. Inman, "Effect of strain nodes and electrode configuration on piezoelectric energy harvesting from cantilevered beams," *J. Vibrat. Acoust.*, vol. 131, no. 1, Feb. 2009, Art. no. 011010.
[38] M. Krishnasamy, F. Qian, L. Zuo, and T. R. Lenka, "Distributed parameter modeling to prevent charge cancellation for discrete thickness piezoelectric energy harvester," *Solid-State Electron.*, vol. 141, pp. 74–83, Mar. 2018.

**TIANYUN GUO** was born in Zhenjiang, China, in 1987. She received the B.E. degree in electrical engineering from Southeast University, Nanjing, China, in 2009, where she is currently pursuing the Ph.D. degree with the School of Electrical Engineering.

From 2012 to 2014, she was a Visiting Scholar with the Department of Electrical Engineering, Virginia Tech, Blacksburg, VA, USA. Her research interests include the design and theoretical modeling of the piezoelectric energy harvesting structures and the development of energy harvesting circuits.

**ZHIKE XU** received the Ph.D. degree from Southeast University, Nanjing, China, in 2005. He is currently an Associate Professor with the School of Electrical Engineering, Southeast University. His research interests include numerical modeling of ultrasonic motors, piezoelectric actuators, and piezoelectric energy harvesting.

**LEI HUANG** received the B.Eng. and M.Eng. degrees from the China University of Petroleum, Dongying, China, in 2002 and 2008, respectively, and the Ph.D. degree from the Southeast University, Nanjing, China, in 2012, all in electrical engineering. He is currently an Associate Professor of electrical engineering with Southeast University. He was a Visiting Scholar with The University of Sheffield, Sheffield, U.K., from 2017 to 2018. His research interests include linear generators, electromechanical energy conversion, and permanent magnet machine.

**MINQIANG HU** received the Ph.D. degree in electrical engineering from the Huazhong University of Science and Technology, Wuhan, China, in 1990. He is currently a Full Professor with the School of Electrical Engineering, Southeast University, Nanjing, China. His research interests include electric machine modeling and simulation, renewable energy generation, distributed generation, and microgrid.

**LONG JIN** received the Ph.D. degree from the Nanjing University of Aeronautics and Astronautics, Nanjing, China, in 1997. He has been a Professor of electrical engineering with Southeast University since 2003. His research interests are in ultrasonic motors, high-power electronics technology, and robot design.

**JIANHUA WANG** (Member, IEEE) received the B.S. and Ph.D. degrees in electrical engineering from the Nanjing University of Aeronautics and Astronautics, Nanjing, China, in 2004 and 2010, respectively.

In 2010, he joined the Faculty of School of Electrical Engineering, Southeast University, Nanjing, where he is currently an Associate Research Professor. He has authored or coauthored more than 40 technical articles. He holds three Chinese patents. His main research interests include MVdc, solid-state transformer, power electronics system stability, distributed generation, and microgrid.